

Research Paper

Differential effects of paramyotonia congenita mutations F1473S and F1705I on sodium channel gating

James R. Groome,^{1,*} Matthew F. Larsen² and Allyson Coonts³

¹Department of Biological Sciences; Idaho State University; Pocatello, Idaho USA; ²Department of Biology; Brigham Young University-Idaho; Rexburg, Idaho USA; ³Department of Biology; Albertson's College; Caldwell, Idaho USA

Key words: charge immobilization, deactivation, fast inactivation, paramyotonia congenita, sodium channel

We investigated effects of paramyotonia congenita mutations F1473S and F1705I on gating of skeletal muscle Na⁺ channels. We used on-cell recordings from *Xenopus* oocytes to compare fast inactivation and deactivation in wild-type and mutant channels. Then, we used gating current recordings to determine how these actions of PC mutants might be reflected in their effects on charge movement and its immobilization. F1473S, but not F1705I, accelerated deactivation from the inactivated state and enhanced the remobilization of gating charge. F1473S and F1705I decreased the completion of closed-state fast inactivation, and decreased charge movement over the voltage range at which channels did not activate. An unexpected result was that F1705I increased the extent of charge immobilization in response to strong depolarization. Our results suggest that the DIV S4-S5 linker mutation F1473S promotes the hyperpolarized position of DIVS4 to accelerate recovery. Inhibition of charge movement by F1473S and F1705I in the absence of channel opening is discussed with respect to their effects on closed-state fast inactivation.

Introduction

Voltage-gated sodium channels regulate electrical signals that characterize the function of excitable cells such as neurons and muscle fibers.^{1,2} Sodium channels in nervous or muscle tissues share a common structure of four domains, each comprised of six transmembrane segments.³ Conserved sequences in these channels promote specific functions. For example, voltage sensitivity is ascribed to the complement of positively charged amino acids in S4 segments⁴⁻⁹ that allow voltage-gated channels to open (activate) or close (deactivate) in response to changes in membrane polarization.

Several determinants of fast inactivation in voltage-gated sodium channels have been identified. The inactivation particle per se has been localized to a conserved IFMT motif in the DIII-DIV linker.¹⁰⁻¹² Other regions of the channel that regulate fast inactivation include the DIVS4 voltage sensor,¹³⁻¹⁵ residues in the S4-S5 linkers of domains III¹⁶ and IV,¹⁷⁻²⁰ S6 segments²¹⁻²³ and the C terminus.²⁴⁻²⁶

Channels opened by strong depolarization subsequently inactivate with kinetics and voltage dependence driven in large part by their coupling to the activation process.^{8,13-14,27-28} Channels subjected to weaker depolarization directly enter the fast-inactivated state without opening.²⁹⁻³⁰ The kinetics of closed-state fast inactivation are relatively slow, as they are not coupled to the rapid kinetics of channel opening.

Channelopathies of skeletal muscle include several forms of non-dystrophic myotonia.³¹⁻³⁴ These include the hyperkalemic and hypokalemic periodic paralyses (PP), potassium-aggravated myotonia (PAM, acetazolamide-responsive, myotonia fluctuans and myotonia permeans) and paramyotonia congenita (PC). Genetic screens of families with PP, PAM, PC or overlap syndromes have revealed numerous point mutations of the *SCN4A* gene encoding the human skeletal muscle sodium channel. Subsequent studies using heterologous expression systems to identify determinants of myotonia or periodic paralysis have linked mutations in *SCN4A* to a spectrum of defects, with some general and noteworthy effects on channel function. Mutant channels in PC were first reported to promote hyperexcitability by slowing entry of channels into the fast-inactivated state, accelerating recovery, and uncoupling fast inactivation from activation.³⁵ PC mutations that disrupt fast inactivation are found in DIVS4,³⁵⁻³⁷ the DIII-DIV linker,³⁸⁻³⁹ the S4-S5 linkers of DIII,⁴⁰ and DIV,^{20,41} as well as the C terminus.⁴²

Other studies have shown that certain PC mutants produce defects in channel deactivation.^{39-40,43-45} Sodium channels exhibit voltage-dependent deactivation from open and inactivated states.⁴⁶ Inactivated-state deactivation, observed as the delay in the onset to recovery, exhibits kinetics that are approximately one order of magnitude slower than those for tail currents observed in open-state deactivation. The relatively slow kinetics of inactivated-state deactivation might be a consequence of gating charge immobilization. Since voltage sensors in DIII and DIV contain the immobilizable fraction of gating charge,⁴⁷ PC mutations in this region of the channel offer a means to study allosteric regulation of voltage sensor movements underlying deactivation. In the present study we compared sodium channel gating parameters in PC mutants F1473S in the DIV S4-S5 linker and F1705I in the C terminus. Whereas open-state deactivation is not affected by these mutations, F1473S accelerates inactivated-state deactivation and recovery from fast inactivation by promoting a rapid remobilization

*Correspondence to: James R. Groome; Department of Biological Sciences; Idaho State University; Pocatello, Idaho 83209-8007 USA; Email: groojame@isu.edu

Submitted: 02/02/08; Revised: 04/03/08; Accepted: 04/07/08

Previously published online as a *Channels* E-publication:
<http://www.landesbioscience.com/journals/channels/article/6051>

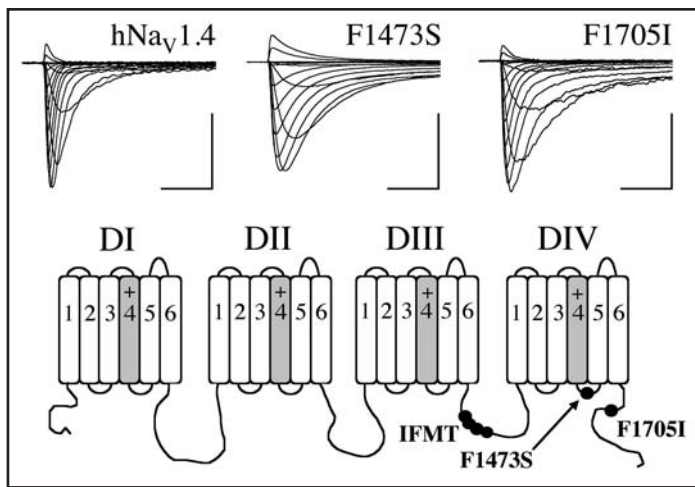


Figure 1. Families of sodium currents in wild-type hNav_v1.4 and PC channels at 12°C. Currents were elicited from -150 mV using 20 ms step commands to voltages ranging from -90 mV to +60 mV. Calibration: 3 ms; hNav_v1.4 and F1705I 300 pA, F1473S 500 pA. Locations of mutations employed in this study are shown in the cartoon depicting the structure of hNav_v1.4.

of the gating charge. F1705I, which lacks the typical PC phenotype of accelerated recovery from fast inactivation, slows the remobilization of gating charge. Both mutants inhibit charge movement in unopened channels, an effect that might contribute to their common action to inhibit closed-state fast inactivation. Some of these results have been reported in abstract form.⁴⁸

Results

Activation. The voltage dependence of activation was measured in the on-cell macropatch configuration by comparing peak current amplitudes for hNav_v1.4 and PC mutants F1473S and F1705I in response to 20 ms depolarizing commands from a holding potential of -150 mV. Families of sodium currents are shown in Figure 1 for step commands to voltages ranging from -90 mV to 60 mV at 12°C. Equilibrium parameters were obtained by fitting the normalized conductance curves (g/V) to Boltzmann distributions. Activation parameters were not dramatically affected by PC mutations. Neither F1473S nor F1705I affected the midpoint of activation, although each significantly increased the slope factor (Table 1). F1473S and F1705I activation kinetics, taken as 10% to 90% of rise time towards peak inward current, were similar to hNav_v1.4 at most voltages tested.

Fast inactivation. Steady-state fast inactivation (h_{∞}) parameters were obtained from experiments in which channels were subjected to 500 ms, variable-voltage pre-pulses prior to test pulses to -20 mV to assess channel availability. The normalized h_{∞} curves were fit to Boltzmann distributions and parameters are listed in Table 1. F1473S and F1705I produced significant shifts of 17.2 mV and 12.7 mV respectively on the midpoint of the h_{∞} curve, without affecting slope factor.

We tested the effects of F1473S and F1705I on open-state fast inactivation kinetics by measuring time constants of current decays in experiments as shown in Figure 1. Compared to hNav_v1.4, fast inactivation was slowed in F1473S and F1705I at voltages more positive than -50 mV or -40 mV respectively (Table 1). τ_{H1} in F1473S

Table 1 **Parameters for hNav_v1.4 and PC channels: On-cell recording configuration**

Gating parameter	hNav _v 1.4	F1473S	F1705I
$V_{1/2}$ (mV)	-32.6 ± 2.3 (20)	-34.2 ± 1.6 (17)	-37.6 ± 1.7 (15)
Slope factor	3.45 ± 0.07 (20)	4.03 ± 0.18 (17)**	3.81 ± 0.06 (15)***
$h_{\infty 1/2}$ (mV)	-86.1 ± 2.2 (20)	-68.9 ± 2.4 (17)***	-73.4 ± 2.3 (15)***
Slope factor	4.11 ± 0.12 (20)	3.76 ± 0.18 (17)	4.27 ± 0.31 (15)
Rise time, 0 mV (ms)	0.33 ± 0.03 (20)	0.40 ± 0.04 (17)	0.33 ± 0.02 (15)
τ_{H1} , 0 mV (ms)	0.92 ± 0.08 (20)	2.55 ± 0.23 (17)***	1.62 ± 0.30 (15)*
τ_{H1} , -80 mV (ms)	29.8 ± 2.6 (10)	32.5 ± 11.0 (12)	116.2 ± 14.1 (13)***
τ_{REC} , -120 mV (ms)	6.42 ± 0.85 (18)	2.13 ± 0.28 (17)***	4.84 ± 0.54 (14)
Recovery delay, -120 mV (ms)	0.98 ± 0.10 (18)	0.37 ± 0.03 (17)***	0.87 ± 0.06 (14)

* $p \leq 0.05$; ** $p \leq 0.01$; *** $p \leq 0.001$; On-cell recording configuration.

was voltage-independent at voltages more positive than -30 mV, resulting in significantly greater values for τ_{H1} compared to F1705I. These effects on fast inactivation for F1473S and F1705I are similar to those reported for these mutations expressed in mammalian cells.^{20,41-42}

Closed-state fast inactivation parameters in hNav_v1.4 and mutant channels were determined from a double pulse protocol. Depolarizations from -90 mV to -50 mV for durations up to 300 ms were delivered to the patch. Immediately following each conditioning pulse, test pulses to -20 mV were used to assess availability of channels (Fig. 2). Decreased responses to -20 mV test pulses during the initial 5 ms (left) and terminal 60 ms (right) of a -70 mV conditioning pre-pulse are shown for hNav_v1.4 and mutant channels in Figure 2A–C. Decreases in normalized current amplitudes over the course of 300 ms pre-pulse duration are shown in Figure 2D. Completion of closed-state fast inactivation was determined from the asymptote, and kinetics determined as the time constant towards completion, from the normalized curves.

F1705I significantly slowed closed-state fast inactivation at all voltages tested, compared to hNav_v1.4 (Fig. 3A). F1473S slowed fast inactivation kinetics following pre-pulses to -60 mV or -50 mV, voltages at which open-state fast inactivation might be expected to contribute to a decrement of current amplitude. Both mutants significantly inhibited the completion of fast inactivation at voltages more negative than -50 mV (Fig. 3B). Since F1705I slowed kinetics of closed-state fast inactivation, we compared completion measurements for this mutation to those obtained in a separate set of 6 measurements using pre-pulse durations up to 500 ms, as used in measurements of steady-state fast inactivation. Asymptotes for F1705I were similar following the 300 ms or 500 ms pre-pulse duration. Taken together, these results indicate that similar actions of F1473S and F1705I on closed-state fast inactivation (less complete) explain their effect on the midpoint of the h_{∞} curve (less likely).

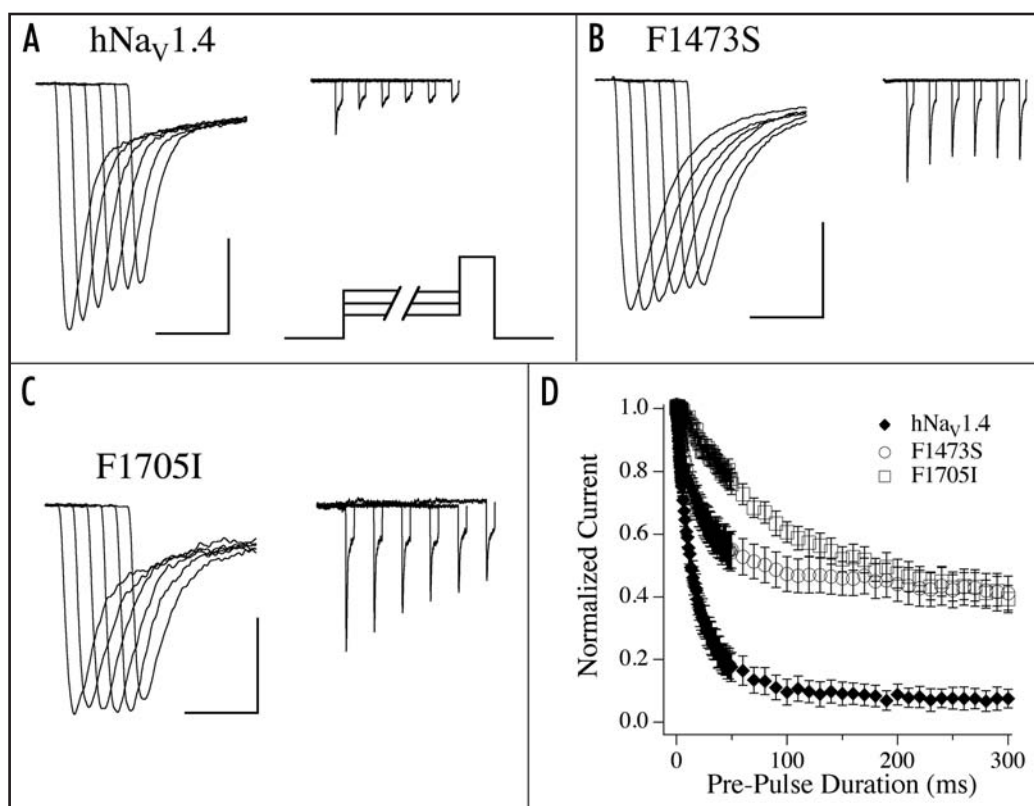


Figure 2. Closed-state fast inactivation in hNav_v1.4 and PC channels. (A–C) Currents obtained in response to -20 mV test pulses for wild-type and PC channels following -70 mV pre-pulses from 0 to 300 ms. At left, currents during the initial 5 ms (every 10th sweep shown); at right, those observed during the terminal 60 ms. Calibration: 5 ms at left, 10 ms at right; hNav_v1.4 and F1473S 500 pA, F1705I 200 pA. (D) Time course of current decreases following -70 mV pre-pulses. Values are mean \pm SEM in 10–12 experiments.

Recovery from fast inactivation was measured from a double pulse protocol used to inactivate and then recover channels in experiments as shown in Figure 4A. As reported for these mutations expressed in mammalian cells,^{20,41} F1473S significantly accelerated the recovery of channels over the voltage range tested of -180 mV to -100 mV (Fig. 4B). Acceleration of recovery in F1473S increased from 1.5-fold compared to hNav_v1.4 at -180 mV, to 3 fold at -120 and -100 mV. Recovery was slightly faster in F1705I compared to hNav_v1.4, but this effect was significant only at -160 mV.

Deactivation. Interpulse intervals in the experiments shown in Figure 4A were stepped in 50 or 100 μ s increments to permit an accurate measurement of the delay in onset to recovery from fast inactivation. Whereas F1705I did not significantly alter delay in the onset to recovery, F1473S significantly abbreviated recovery delay at all voltages tested (Fig. 4C). Recovery delay in F1473S was consistently 2-fold shorter in duration than hNav_v1.4.

We then tested F1473S and F1705I for effects on deactivation from the open state with tail current measurements. Channels were opened with brief 50 mV pulses prior to commands from -180 mV to -70 mV to elicit tail currents. PC mutations slightly prolonged tail current decay at voltages more positive than -90 mV when 0.5 ms pulses were used to open channels (Fig. 5A). To control for the possibility that fast inactivation might influence tail currents, we repeated these experiments with 0.2 ms or 0.1 ms pulse durations (Fig. 5B and C). With shorter pulses used to open channels, deactivation time constants were unaffected by either F1473S or F1705I compared to

hNav_v1.4, indicating that neither mutation altered open-state deactivation. Thus, F1473S accelerates the deactivating transition only in channels that have fast inactivated.

Gating charge movement. State transitions in voltage-gated channels are promoted by charge movement with S4 translocation. We compared Q/V relations, gating charge immobilization and its remobilization in wild-type and PC channels to determine if gating defects in F1473S and F1705I are the consequence of altered voltage sensor movements. Immobilization of the gating charge occurs with fast inactivation of the channel.²⁷ We hypothesized that slowed fast inactivation in these mutations would parallel a slowed onset of gating charge immobilization, and decrease its extent. Recovery of channels that have fast-inactivated is predicted by remobilization of gating charge in DIVS4.⁵⁰ F1473S, but not F1705I, accelerated recovery from fast inactivation and shortened the delay in onset to recovery. Therefore, we also hypothesized that remobilization of the gating charge would be faster in F1473S, but not in F1705I.

Outward ionic currents in the cut-open configuration were elicited from a -120 mV holding potential by step depolarizations from -90 mV to +60 mV (Fig. 6A). Ionic current was blocked with 2 μ M tetrodotoxin (TTX, Fig. 6B). Gating charge movement (Fig. 6C) was quantified by calculating the integrals from ON gating currents ($I_{G_{ON}}$). Normalized measurements of ionic current (I/I_{MAX}) and gating charge (Q/Q_{MAX}) are shown in Figure 6D. Each of these curves was fit to a Boltzmann distribution and parameters are given in Table 2. F1705I produced a significant, 6.3 mV shift of the

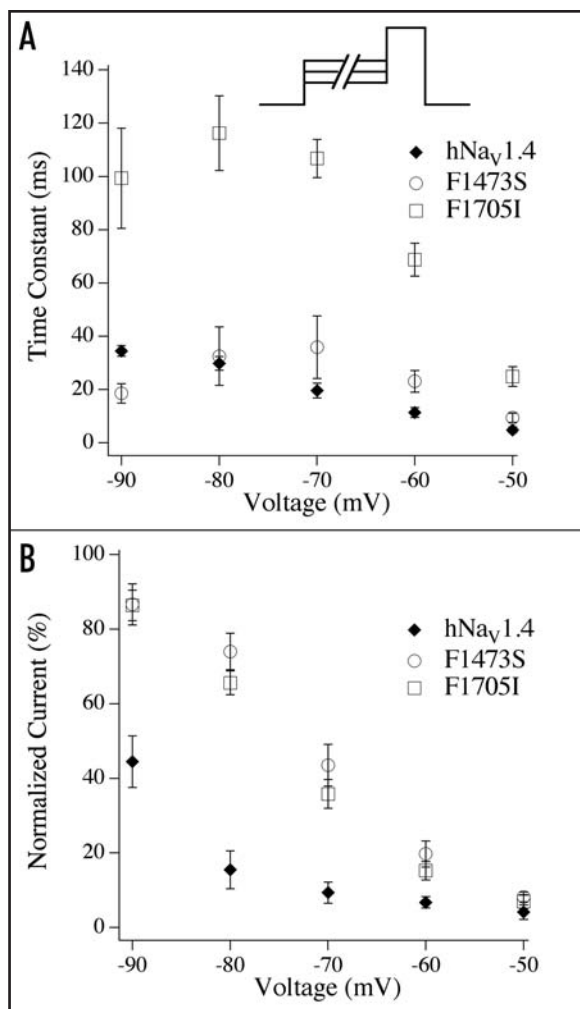


Figure 3. (A) Kinetics of closed-state fast inactivation for hNav_v1.4, F1473S and F1705I over the pre-pulse voltage range of -90 mV to -50 mV. (B) Percent of initial current remaining in response to test pulses after 300 ms pre-pulses to the voltage shown in these same experiments. Values are mean \pm SEM for 10–16 experiments.

midpoint of the I/V curve, without affecting slope factor. In contrast to their modest effects on activation, PC mutants produced more obvious effects on charge movement. The midpoint of the Q/V curve was significantly shifted by F1473S (15.5 mV) and F1705I (25.9 mV), and F1473S also decreased the slope factor.

The I/V curves in Figure 6 show that wild-type and mutant channels activated with a threshold between -40 mV and -30 mV. Whereas hNav_v1.4 exhibited, as expected, substantial charge (Q/Q_{MAX}) movement at activation threshold or at more negative voltages, PC channels inhibited charge movement over this voltage range. At -40 mV, $37.2 \pm 2.4\%$ of the maximum charge movement (Q/Q_{MAX}) was reached in hNav_v1.4 (Table 2). In contrast, PC mutations limited charge movement at sub-threshold voltages. At -40 mV, Q/Q_{MAX} values in F1473S ($22.1 \pm 2.0\%$) and in F1705I ($13.1 \pm 3.0\%$) were significantly decreased compared to hNav_v1.4.

Gating charge immobilization. To compare the extent of charge immobilized in hNav_v1.4 and PC channels, we measured total ON and fast OFF integrals from gating currents in response to step depolarizations as shown in Figure 7A. Charge immobilization was

calculated as $1 - (I_{G_{OFF\ FAST}}/I_{G_{ON}})$ and plotted against membrane potential (Fig. 7B). Immobilization curves were fit to Boltzmann distributions and parameters are given in Table 2. Similar to their effect on the Q/V curve, F1473S and F1705I significantly shifted the midpoint of the immobilization curve by 26.4 mV and 26.5 mV, and F1473S also decreased slope factor. F1473S decreased charge immobilization at voltages more negative than 20 mV. F1705I produced a biphasic effect, significantly decreasing charge immobilization over the voltage range from -60 mV to -20 mV, but increasing charge immobilization at voltages more positive than -10 mV.

We determined the onset of charge immobilization by comparing $I_{G_{ON}}$ and $I_{G_{OFF\ FAST}}$ in response to variable-voltage and duration depolarizations, as shown in Figure 8. Percent charge immobilized was determined for each time point. For hNav_v1.4 and PC mutants, the resulting curves were best fit with double exponential functions at -40 mV, whereas curves from more depolarized pulses were best fit with single exponential functions. Time constants for onset of charge immobilization were then compared to the kinetics of fast inactivation of unblocked channels in the cut-open recording configuration (Fig. 9). Charge immobilized at a rate more rapid than the entry of channels into the fast-inactivated state. F1473S produced voltage-independent fast inactivation and gating charge immobilization at more depolarized potentials.

Recovery from charge immobilization was studied with a double pulse protocol. 0 mV depolarizations were used to promote the initial $I_{G_{ON}}$, and recovering $I_{G_{ON}}$ following interpulse voltages ranging from -100 mV to -70 mV (Fig. 10). In the fast phase of recovery, F1473S significantly increased, and F1705I decreased, the extent of charge remobilized compared to hNav_v1.4. Over this range of interpulse intervals, the extent of charge remobilized in hNav_v1.4 ($43.1 \pm 1.0\%$), F1473S ($61.9 \pm 6.2\%$) and in F1705I ($24.2 \pm 2.1\%$) was similar to the magnitude of gating charge not immobilized at 0 mV, as determined from experiments as shown in Figure 7B. These findings support the notion that the initial rise in gating charge recovered is due to S4 translocation unimpeded by charge immobilization.

Gating charge recovery proceeded with a bi-exponential time course (Fig. 10). F1705I did not alter the kinetics of either phase of remobilization. F1473S slowed the kinetics of the initial phase at -70 mV and -80 mV but significantly accelerated the second phase of gating charge recovery (Table 2). Thus, F1473S enhanced the return of the gating charge by increasing its extent (fast phase) and accelerating the rate of remobilization (slow phase).

Discussion

Sodium channel dysfunction in non-dystrophic myotonia has been studied using heterologous expression systems to elucidate common gating defects that might explain muscle fiber hyperexcitability. Studies of PC mutations have also yielded valuable insight into the structural determinants of sodium channel gating. In the present study we investigated the effects of PC mutants F1473S and F1705I, with a focus on deactivation, charge movement and its immobilization. We found that F1473S and F1705I, expressed in oocytes, produce effects on gating parameters similar to effects reported in mammalian expression systems. Both mutants slow the entry of channels into the fast-inactivated state, and inhibit closed-state fast inactivation. Whereas neither mutation alters deactivation of channels from the open state, F1473S accelerates inactivated-state

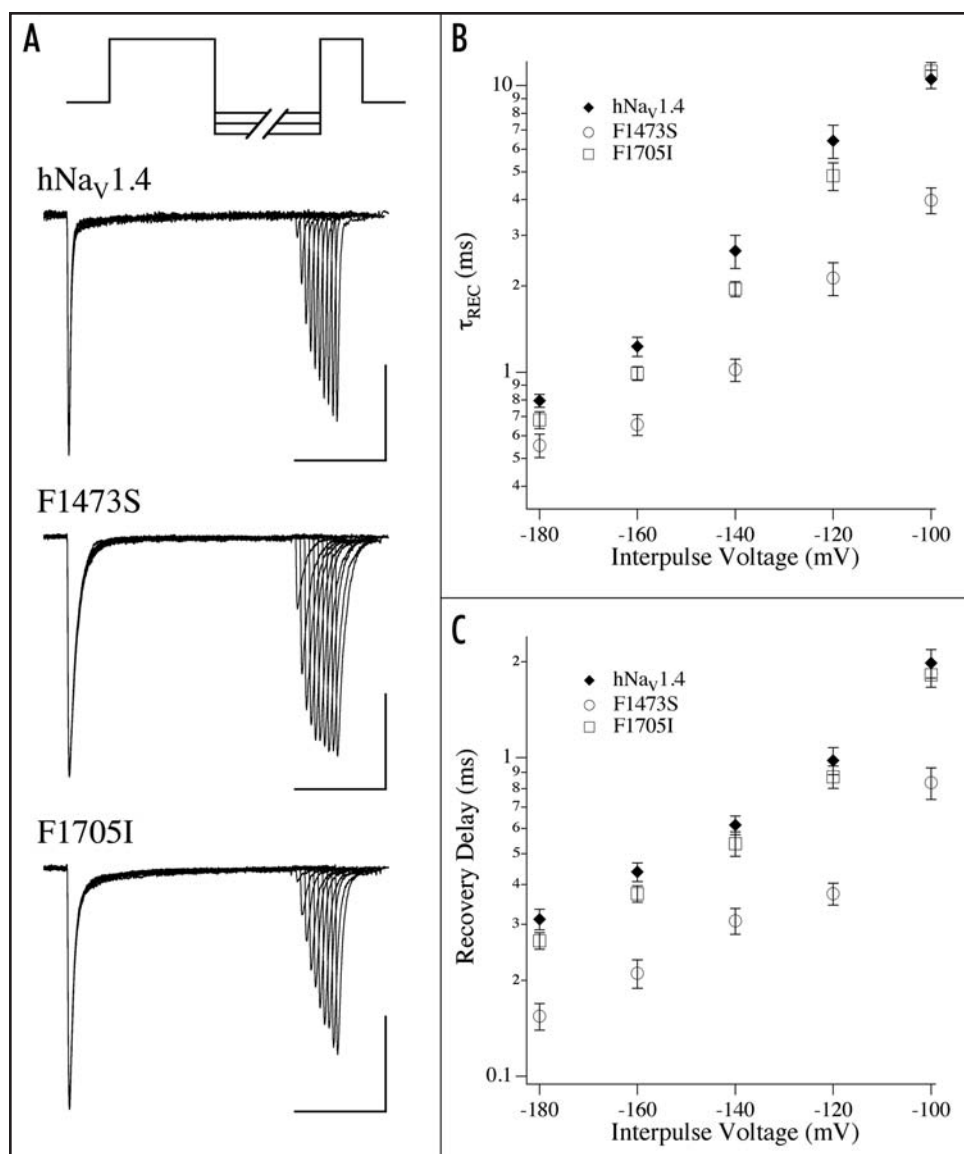


Figure 4. Recovery from fast inactivation in hNav_v1.4 and PC channels. A. Double pulse protocol used to generate recovery currents shown at 1 ms intervals (every 10th sweep shown) following variable-duration, -120 mV interulses. Calibration: 10 ms; hNav_v1.4 200 pA, F1473S and F1705I 500 pA. Values for voltage dependence of recovery (B) and recovery delay (C) are mean \pm SEM for 14–18 experiments.

deactivation to promote faster recovery. These effects of F1473S are predicted by its effect to enhance the remobilization of charge in fast inactivated channels. At voltages negative to activation threshold, the extent of charge and its immobilization were significantly decreased in PC mutants. At more depolarized voltages, F1705I produced the unexpected result of increasing the immobilizable fraction of the gating charge compared to wild-type channels.

Comparison of F1473S and F1705I; open-state fast inactivation. The PC mutation F1473S is located in the DIV S4-S5 linker.³¹ Fast inactivation is slowed by F1473S,^{20,41} (and see Table 1) by the homologous mutation F1661S in severe myoclonic epilepsy of infancy⁵¹ and by analogous mutations at this residue.^{18,19,52-53} Cysteine scanning mutagenesis of residues in the DIV S4-S5 linker in Na_v1.4 suggests an α helical structure.^{18,52} F1473 and other residues in the proximal region of the linker are accessible

to sulfhydryl reagents at depolarized as well as hyperpolarized membrane potentials. These findings suggest that residues distal to F1473 likely comprise the IFMT receptor itself.^{18-20,52-53}

In response to membrane depolarization, movement of DIVS4 promotes fast inactivation,⁵⁴⁻⁵⁵ probably by exposing a binding site for the IFMT motif. That action supports a model in which DIVS4 couples the voltage dependencies of activation and fast inactivation.^{7,8,13,14} Mutations at residues analogous to F1473, A1474, M1476 and M1477 in the DIV S4-S5 linker typically reduce the voltage dependence of fast inactivation,^{17,56} and suggest that F1473 comprises a portion of the molecular link coupling voltage-dependent activation to fast inactivation. In the present study we found that F1473S reduced the voltage dependence of fast inactivation, the extent of charge immobilized and the kinetics of charge immobilization. Our results thus support previous studies suggesting that this residue helps co-ordinate activation/inactivation coupling. In addition, they suggest a role for F1473 in the coupling of activation to immobilization of gating charge in DIVS4.

F1705I is located in the C terminus,⁴² a region recently identified as a determinant of sodium channel fast inactivation.²⁴⁻²⁶ While F1705I produced significant slowing of fast inactivation, the voltage dependence of fast inactivation and of charge immobilization in F1705I were similar to hNav_v1.4, unlike F1473S. In addition, only F1705I increased charge immobilization at voltages for which channels open and then inactivate. To our knowledge this is the first report of a sodium channel mutation that increases charge immobilization compared to the wild-type channel. Differential effects of F1473S and F1705I on gating charge movement in response to strong depolarization suggest to us that these two PC mutants are unlikely to promote their overtly similar actions to slow open-state fast inactivation by identical mechanisms. A previous report⁴² suggests the possibility that F1705I might disrupt fast inactivation in a manner like that of the nearby GEFS⁺ type II mutation D1866Y in Na_v1.1 by inhibiting interaction of the C termini of α and β subunits.⁵⁷ Additional studies are needed to identify the molecular mechanisms by which C terminal mutations disrupt fast inactivation and to determine the role of this region of the channel in charge immobilization.

Charge movement and closed-state fast inactivation. We found that F1705I slows fast inactivation at voltages for which channels do not open, unlike F1473S. In contrast to these disparate effects on kinetics, both mutations decrease the completion of closed-state fast

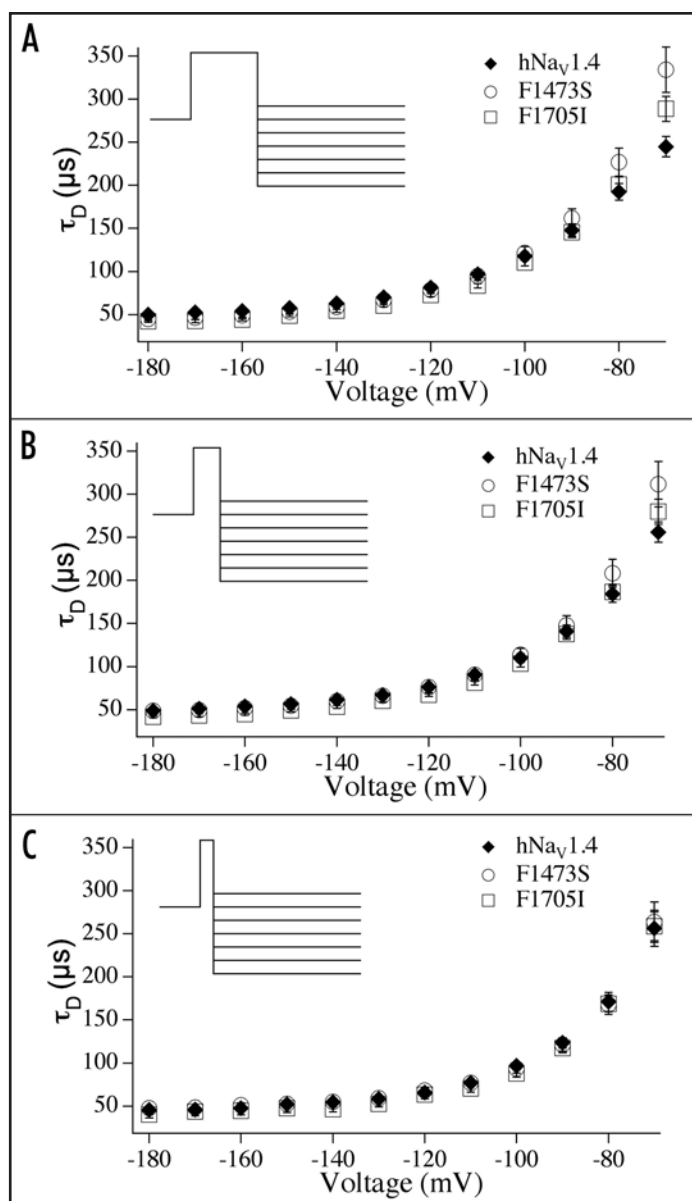


Figure 5. Open-state deactivation determined from tail currents. Channels were briefly opened to 50 mV for durations ranging from 0.5 ms (A), 0.2 ms (B) or 0.1 ms (C) prior to hyperpolarizing commands to the voltages shown. Values are mean \pm SEM in 12–20 experiments.

inactivation. Therefore, incomplete closed-state fast inactivation, rather than slowed kinetics, explains the similar depolarizing shift produced by F1473S and F1705I on the steady-state fast inactivation curve.

An examination of the normalized Q/V and I/V curves from experiments utilizing the cut-open oocyte clamp reveals that significant charge moves in wild-type channels at voltages more negative than the threshold of activation. Thus, a “window potential” is observed for which charge movement occurs in the absence of channel activation. Both F1473S and F1705I produced a significant depolarizing shift of the Q/V curve and decrease this window of potential between gating and ionic current. The decrease in gating charge movement at sub-threshold potentials was paralleled by a decrease in the extent of immobilized charge and of inactivation,

suggesting a possible common link. Interestingly, gating charge immobilization and closed-state fast inactivation are causally related in $K_{V4.2}$ channels.⁵⁸

It has been postulated that for weak depolarizations that do not open the activation gate, DIIIS4 and DIVS4 voltage sensors promote inactivation from the closed state.³⁰ While our results do not yet present a molecular mechanism for closed-state fast inactivation, our results set the stage for future studies examining the relative contributions of DIIIS4 and DIVS4 voltage sensor movements to inactivate closed channels.

Charge immobilization and deactivation. Our results suggest that the most significant effect of F1473S on sodium channel recovery is to enhance the remobilization of the gating charge in inactivated channels. This mutation abbreviated inactivated-state deactivation without altering deactivation of channels from the open state. F1473S significantly reduced the extent of gating charge immobilized at 0 mV, the potential used in recovery protocols in the on-cell and cut-open recording configurations. We propose that decreased charge immobilization in F1473S dictates the more rapid return of channels to an available state, and accelerates recovery. Nevertheless, we found that F1473S produced effects on recovery rate not perfectly correlated with effects on recovery delay over the range of interpulse voltages tested. In addition, whereas F1705I did not affect recovery or its delay, charge immobilization was increased. Therefore, effects of the mutants of the recovery of channels from fast inactivation may only be fully explained with an examination of putative effects downstream of the deactivation transition, such as unbinding of the IFMT motif.

We found that gating defects of F1473S and F1705I, expressed in oocytes, are similar to those described for these mutations expressed in mammalian cells. Our use of oocytes to study these channels allowed us to measure gating charge movement and its immobilization with the cut-open oocyte recording configuration. F1473S and F1705I each decrease the completion of closed-state fast inactivation, and reduce charge immobilization at voltages for which channels do not open. In addition, F1473S and F1705I produce effects on recovery from fast inactivation generally paralleled by their effects on the remobilization of charge. However, it should be noted that a causal link of altered charge movement or its immobilization in F1473S and F1705I to the cellular phenotype of myotonia remains to be determined.

Materials and Methods

Site-directed mutagenesis. Mutations F1473S and F1705I were made from template *SCN4A* in SP64T vector with PCR-directed mutagenesis using Quik-Change II XL Site Directed Mutagenesis Kits™ (Stratagene, La Jolla, CA). All constructs were confirmed by sequencing. Plasmids were linearized with *NotI* and transcribed with T7 RNA polymerase for injection into oocytes.

Oocyte preparation. *Xenopus laevis* oocyte lobes were surgically removed after anesthetizing the animals with 0.17% tricaine (3-aminobenzoic acid ethyl ester, Sigma, St. Louis, MO) according to guidelines approved by Animal Use and Care Committees at ISU. Oocytes were isolated by defolliculation after 10 min exposure to 2 mg/mL collagenase in a solution containing (in mM): NaCl 96, KCl 2, MgCl₂ 20, HEPES 5, pH 7.4. Culture of oocytes was done at 18°C in medium containing (in mM): NaCl 96, KCl 2, MgCl₂ 1,

Table 2 Parameters for hNa_v1.4 and PC channels: Cut-open oocyte recording configuration

Gating parameter	hNa _v 1.4	F1473S	F1705I
I/V _{1/2} (mV)	12.4 ± 1.7 (15)	11.2 ± 0.9 (13)	6.2 ± 2.0 (13)*
Slope factor	1.65 ± 0.08 (15)	1.53 ± 0.05 (13)	1.70 ± 0.07 (13)
Q/V _{1/2} (mV)	-33.6 ± 1.5 (13)	-18.1 ± 3.7 (12)**	-7.7 ± 6.7 (8)**
Slope factor	1.80 ± 0.07 (13)	1.13 ± 0.11 (12)***	1.94 ± 0.28 (8)
Q/Q _{MAX} , -40 mV	0.37 ± 0.02 (13)	0.22 ± 0.02 (12)***	0.13 ± 0.05 (8)***
% Charge immobilized V _{1/2}	-53.3 ± 3.0 (13)	-26.9 ± 7.6 (12)**	-26.8 ± 4.5 (8)***
Slope factor	390.5 ± 42.0 (13)	233.0 ± 59.8 (12)*	364.7 ± 61.5 (8)
τ _H , inactivation at 0 mV (ms)	1.74 ± 0.18 (15)	4.81 ± 0.32 (13)***	3.29 ± 0.23 (13)**
τ _{ON} , immobilization at 0 mV (ms)	1.26 ± 0.11 (11)	1.61 ± 0.30 (10)	1.78 ± 0.31 (13)
τ _{REC FAST} , -80 mV (ms)	1.11 ± 0.12 (11)	2.67 ± 0.58 (12)*	0.80 ± 0.18 (13)
τ _{REC SLOW} , -80 mV (ms)	29.9 ± 4.7 (11)	15.0 ± 4.4 (12)*	29.2 ± 5.2 (13)

*p ≤ 0.05; **p ≤ 0.01; ***p ≤ 0.001; Cut-open recording configuration.

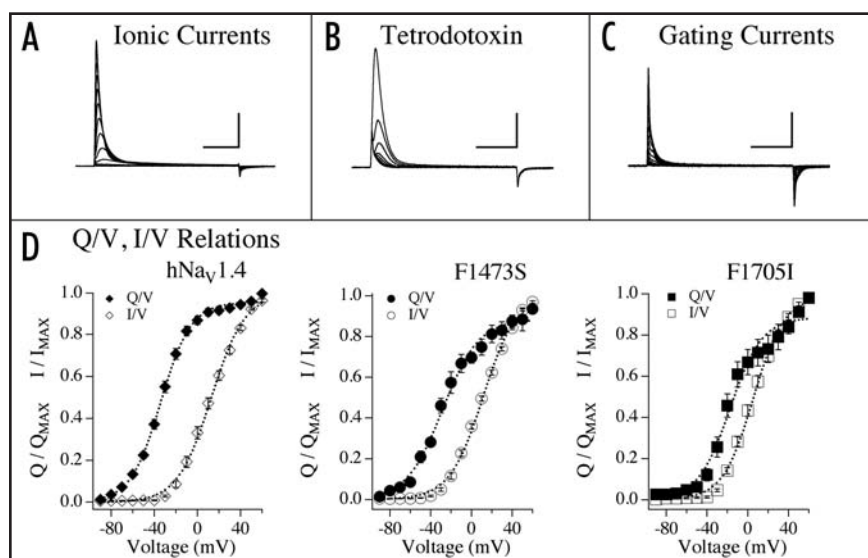


Figure 6. Ionic and gating currents in the cut-open configuration. Outward ionic currents in response to step commands from -120 mV are shown in (A). Ionic currents were blocked by 2 μM TTX (B), resulting in gating currents shown in (C). Calibration: 5 ms; (A) 1.5 μA, (B) 1 μA, (C) 200 nA, (D) I/V and Q/V relations for hNa_v1.4 and PC channels. Values are mean ± SEM in 8–15 experiments.

CaCl₂ 1.8, HEPES 5, sodium pyruvate 2.5, pH 7.4, with 100 mg/l gentamicin and 3% horse serum (Hyclone Laboratories, Logan, UT). Oocytes were co-injected with mRNA for sodium channel α and β₁ subunits (1:1 volume, α subunit at 1 μg/μl, β₁ subunit at 3 μg/μl) in a volume of 50 nl/oocyte.

Macropatch recordings. On-cell macropatch recordings were used to obtain data shown in Figures 1 to 5. The bath solution contained (in mM): NaCl 9.6, KCl 88, EGTA 11, HEPES 5, pH 7.4 and recording pipette solution contained (in mM): NaCl 96, KCl 4, MgCl₂ 1, CaCl₂ 1.8, HEPES 5, pH 7.4. Recordings were done using EPC-9 or EPC-10 patch-clamp amplifiers (HEKA, Lambrecht, Germany) controlled via Pulse or PatchMaster™ software (HEKA) run by Macintosh G4 or G5 computers. Bath solution was maintained at 12°C with a Peltier device and HCC-100A temperature controller (Dagan Corporation, Minneapolis, MN). We performed experiments at 12°C to slow deactivation kinetics

for better resolution, and preliminary experiments indicated that gating parameters exhibited sensitivity to decreased temperature for which 12°C was not saturating. Oocyte holding potential was -120 mV between trials and changed to -150 mV immediately prior to each protocol. Leak (p/4) and capacitance subtractions were done following patch formation and corrected before each voltage clamp experiment. Analyses and graphing were done using PulseFit (HEKA) and Igor Pro 6.0 (WaveMetrics, Lake Oswego, OR).

Equilibrium parameters were obtained from responses to variable-voltage, 20 ms test pulses from -150 mV (activation), or in response to -20 mV test pulses following variable-voltage, 500 ms pre-pulses (inactivation). Conductance/voltage (g(V)) relationships were derived using Equation 1:

$$g_{Na} = I_{max}/(V_M - E_{Na}) \quad \text{Eqn. 1}$$

where g_{Na} is sodium conductance, I_{max} is calculated as peak current in response to the test pulse, V_M is test pulse voltage, and E_{Na} is the measured Na⁺ equilibrium potential. Steady-state activation and fast inactivation (h_{∞}) curves were fit to Boltzmann distributions according to Equation 2:

$$(I/I_{max}) = 1/(1 + \exp(-ze_0(V_M - V_{1/2})/kT)) \quad \text{Eqn. 2}$$

where the normalized current amplitude I/I_{max} is measured from the response to the test pulse potential V_M , z is the apparent valence, e_0 is elementary charge, $V_{1/2}$ is midpoint voltage, k is the Boltzmann constant, and T is temperature in K.

We measured activation kinetics as the time for 10% to 90% of peak inward current in experiments as shown in Figure 1. We measured kinetics of fast inactivation from the open and closed states, and for recovery. Time constants of open-state fast inactivation were determined by fitting current decays to Equation 3:

$$I(t) = \text{offset} + a_1 \exp(-t/\tau_H) \quad \text{Eqn. 3}$$

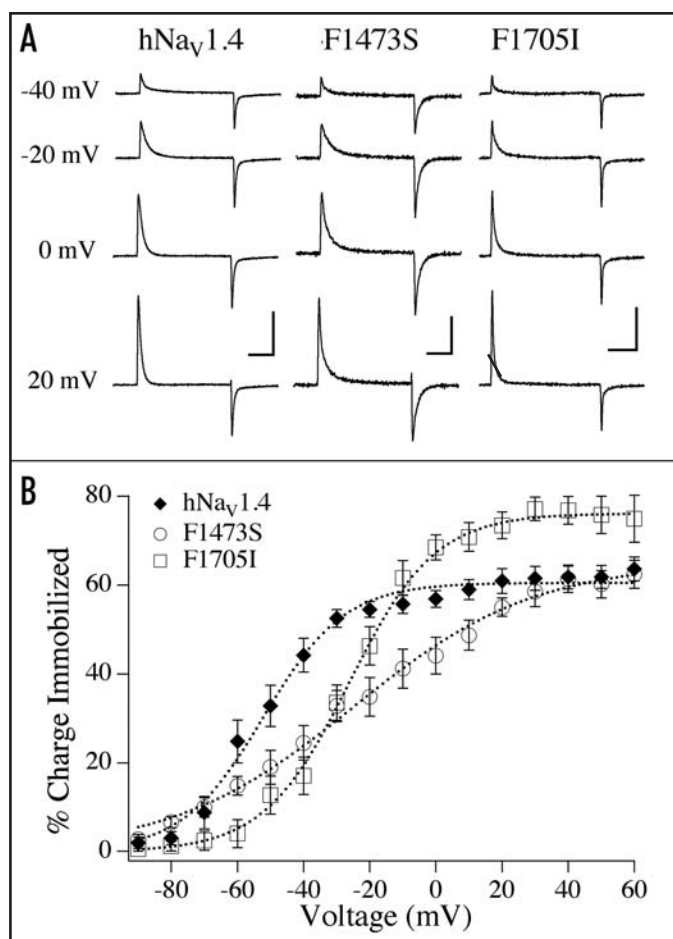


Figure 7. Charge immobilization in hNav_v1.4 and PC channels. (A) Traces are I_{gON} and I_{gOFF} in response to step commands to the voltages shown. Calibration: 5 ms; hNav_v1.4 and F1705I 200 nA, F1473S 100 nA. (B) Voltage dependence of % charge immobilized. Values are mean \pm SEM in 8–13 experiments.

where offset is plateau amplitude, a_1 is current amplitude at $t = 0$, and τ_H is the time constant. Kinetics and completion of closed-state fast inactivation were determined from experiments utilizing a double pulse protocol. First, channels were subjected to pre-pulses at voltages ranging from -90 mV to -50 mV for durations up to 300 ms. Pre-pulses were applied in three contiguous segments in which durations ranged from 0 to 5 ms, 5 to 50 ms and 50 to 300 ms. During the second (test) pulse, channels were subjected to 20 ms, -20 mV test pulses to assess channel availability. Decreases in peak current amplitude were normalized to the response to the initial test pulse, and the normalized curve over 300 ms was fit with Equation 3 to determine τ_H . Completion of fast inactivation from the closed state was assessed from the asymptote (offset) of the normalized curve and expressed as % normalized current.

Recovery from fast inactivation was measured using a double pulse protocol in which 0 mV, 50 ms depolarizing pulses to inactivate channels were followed by interpulses at voltages from -180 mV to -100 mV, at durations ranging from 0 to 10 ms. Channel availability was assessed after each interpulse interval with a second depolarization to 0 mV. Peak amplitudes of recovery currents were normalized to the initial depolarization for that sweep, and recovery

time constants were calculated from single exponential fits to recovery curves according to Equation 3 with the parameters:

$$I(t) = \text{offset} + a_1 \exp(-t/\tau_{\text{REC}})$$

where offset is plateau amplitude, a_1 is current amplitude at $t = 0$, and τ_{REC} is the time constant. From these same experiments we calculated the kinetics of inactivated-state deactivation. To do this we extrapolated peak amplitudes of normalized recovery currents to the time for zero current, from the above equation. That time, the delay in the onset to recovery from fast inactivation, was taken for kinetics for inactivated-state deactivation.^{44,46} Open-state deactivation kinetics, given as time constants (τ_D), were derived from the decay of tail currents. Channels were briefly opened with a depolarization to 50 mV prior to command hyperpolarizations at voltages from -180 mV to -70 mV, and τ_D was determined using equation 3 with the following parameters:

$$I(t) = \text{offset} + a_1 \exp(-t/\tau_D)$$

where $I(t)$ is current amplitude as a function of time, offset is plateau amplitude, a_1 is current amplitude at $t = 0$, and τ_D is the deactivation time constant.

Cut-open oocyte recordings. Sodium channel gating currents were recorded using the cut-open oocyte clamp as described earlier.⁴⁹ Briefly, top and middle (guard) chambers were filled with external gating solution (in mM): NMG-MES (N-methyl D-glucamine, methanesulfonic acid) 120, HEPES 10, Ca(OH)₂ 2, pH 7.4. The bottom chamber was filled with internal gating solution (in mM): NMG-MES 120, HEPES 10, EGTA 2, pH 7.4. Glass electrodes containing platinum wires and filled with 3% agar in 500 mM NMG-MES connected each pool to a CA-1B amplifier (Dagan) via salt bridges with 1 M NaCl. Electrical access to the interior of the oocyte was obtained by rinsing the bottom chamber with 0.5% saponin in internal solution. The animal pole was impaled with a borosilicate electrode filled with 3 M KCl, and membrane potential clamped to -100 mV.

Ionic currents were elicited with commands from a holding potential of -120 mV (Fig. 6A). Gating currents (Fig. 6C) were isolated by adding 2 μ M tetrodotoxin (TTX, Sigma) to the upper chamber, followed by a train of 20 ms step depolarizations to 0 mV. I/V relations were determined from peak amplitudes of outward current in response to commands to voltages from -90 mV to 60 mV. Q/V relations were determined by integrating total outward gating currents (I_{gON}) to quantify charge movement over that voltage range. Normalized curves for I/I_{MAX} and Q/Q_{MAX} were fit to Boltzmann distributions according to equation 2 to obtain equilibrium parameters.

Immobilization of the gating charge was measured by integrating the fast component of the inward gating current ($I_{gOFF \text{ FAST}}$) at the end of each step depolarization, and comparing to I_{gON} according to Equation 4:

$$\% \text{ charge immobilized} = 1 - (I_{gOFF \text{ FAST}}/I_{gON}) \quad \text{Eqn. 4}$$

Percent of charge immobilized was plotted against command voltage and the resulting curves were fit to Boltzmann distributions

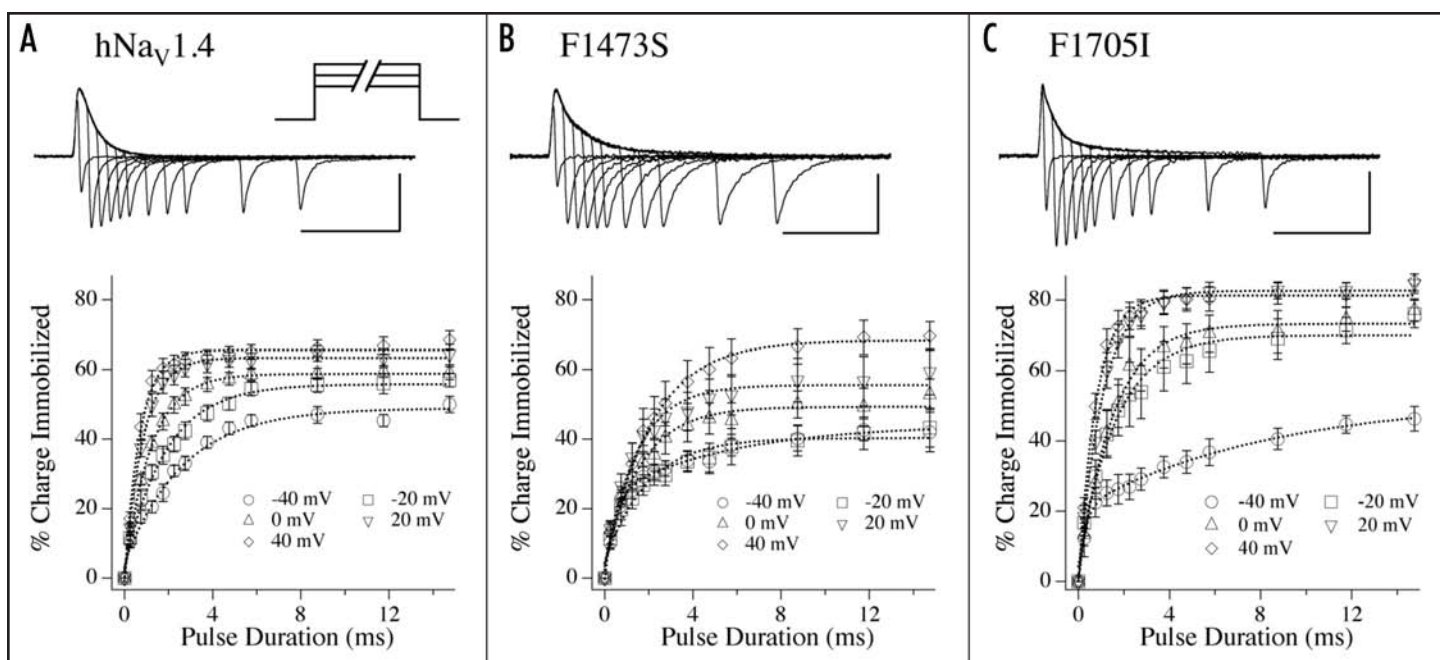


Figure 8. Onset of charge immobilization in hNa_v1.4 and PC channels. From a holding potential of -120 mV, variable-voltage and duration pulses were applied to generate I_{gON} and I_{gOFF} as shown at top. Calibration: 5 ms; F1473S 150 nA, hNa_v1.4 200 nA, F1705I 250 nA. For each plot of time course of charge immobilization, values are mean \pm SEM for 8–14 experiments.

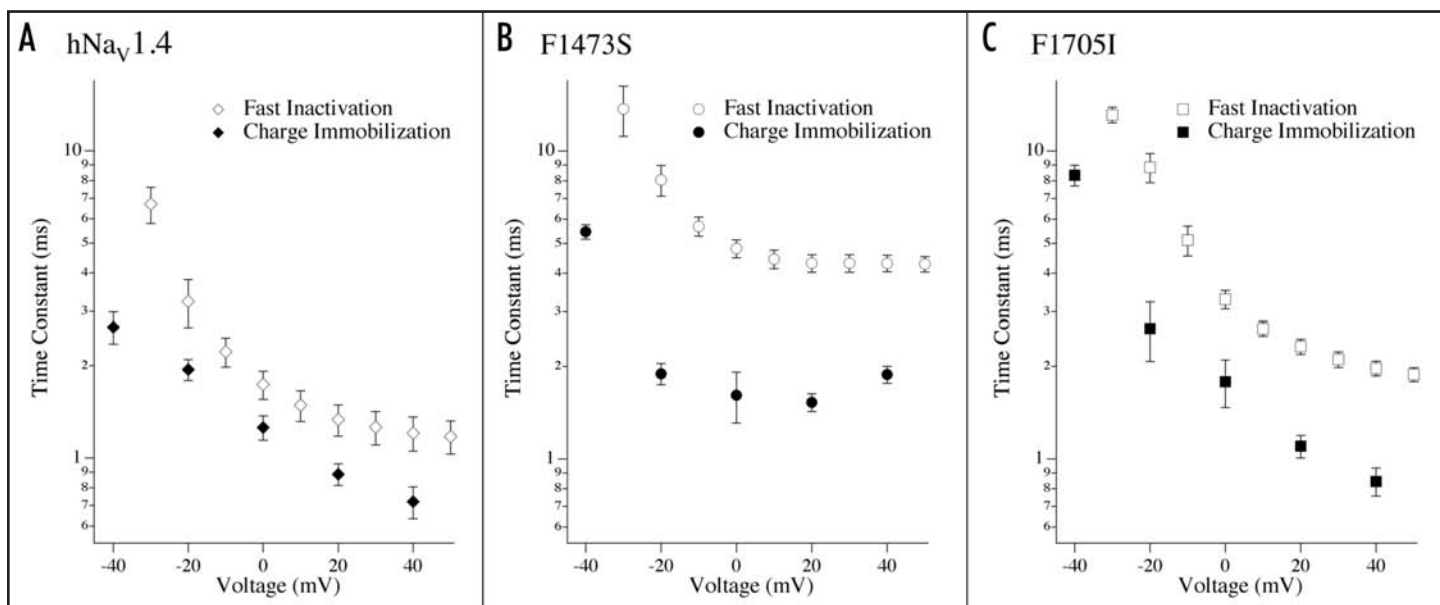


Figure 9. Comparison of kinetics of open-state fast inactivation (open symbols) to onset of charge immobilization (closed symbols). Kinetics of fast inactivation were derived from single exponential fits to decays of ionic current. Kinetics of charge immobilization were calculated from the curves shown in Figure 8 as the slow component of a double exponential (-40 mV) and from single exponential fits at all other voltages. Values are mean \pm SEM for 8–15 experiments.

according to equation 2 to obtain equilibrium parameters for charge immobilization.

Onset kinetics of gating charge immobilization were determined from experiments using variable-duration (0 to 15 ms) pulses at voltages from -40 mV to 40 mV, using equation 4. We determined kinetics at each voltage by fitting the % charge immobilized curve to a single exponential function, using equation 3. Kinetics at -40 mV fit more closely with a double exponential function (see Eqn. 5).

Recovery, or remobilization of gating charge, was determined in experiments using a double pulse protocol. The membrane was depolarized to 0 mV for 30 ms to inactivate channels and immobilize the gating charge. Interpulses at voltages ranging from -100 mV to -70 mV for durations up to 50 ms were followed by a second depolarization to 0 mV to assess recovery of the gating charge. Integrals for I_{gON} following interpulse commands were normalized to the initial I_{gON} , and remobilization parameters determined by fitting the recovery curve with Equation 5:

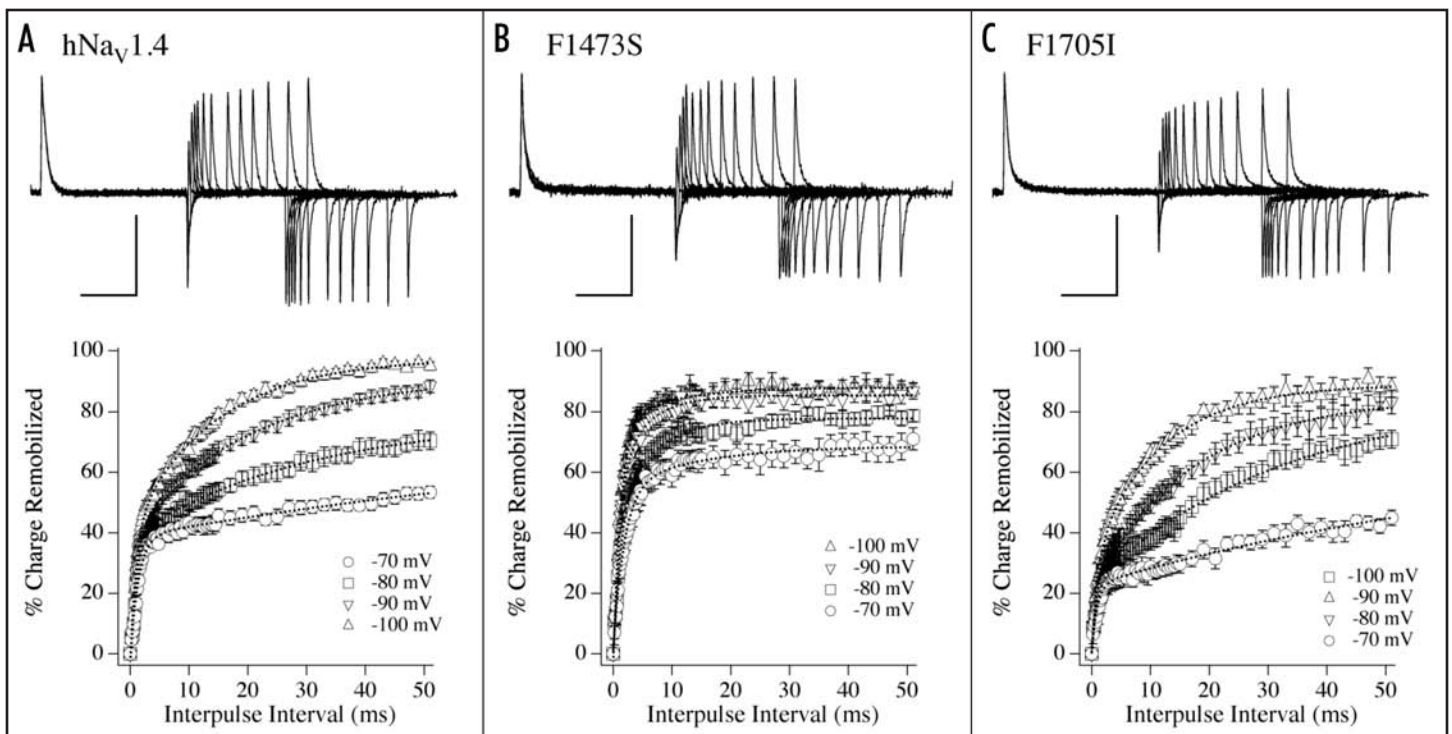


Figure 10. Remobilization of the gating charge. A double pulse protocol was used to generate initial and recovering I_{gON} as shown by the traces (selected sweeps) shown at top. Calibration: 10 ms; F1473S 150 nA, hNa_v1.4 and F1705I 200 nA. For each plot of time course of gating charge remobilization, values are mean \pm SEM for 10–13 experiments.

$$I_g(t) = \text{offset} + a_1 \exp(-t/\tau_{\text{recF}}) + a_2 \exp(-t/\tau_{\text{recS}}) \quad \text{Eqn. 5}$$

where $I_g(t)$ is the normalized I_{gON} as a function of time, offset is plateau amplitude, a_1 and a_2 are asymptotes for the fast (F) and slow (S) phases of recovery, and τ_{recF} and τ_{recS} are time constants.

Statistical significance was assessed with InStat 2.0 (GraphPad, San Diego, CA) using Student's unpaired "t" tests or, where there was a statistically significant difference between standard deviations, Welch's alternative "t" tests. Statistical significance of difference between hNa_v1.4 and mutations was accepted at $p \leq 0.05$.

Acknowledgements

We would like to thank Dr. Katarina Stroffekova (Utah State University, Logan, UT) and Jennifer Abruzzese (University of Utah, Salt Lake City, UT) for their comments on a draft of this manuscript, and Esther Fujimoto (University of Utah) for help with molecular biology. This work was supported by NSF RUI 023558 to James R. Groome and by NIH P20 RR016454 to Idaho State University.

References

1. Armstrong CM, Hille B. Voltage-gated ion channels and electrical excitability. *Neuron* 1998; 20:371-80.
2. Catterall WA. From ionic currents to molecular mechanisms: the structure and function of voltage-gated sodium channels. *Neuron* 2000; 26:13-25.
3. Noda M, Shizimu S, Tanabe T, Takai T, Kayano T, Ikeda T, Takahashi H, Nakayama Y, Kanaoka N, Minamino N, Kangawa K, Matsuo K, Raftery H, Hirose M, Inayama T, Hayashida H, Miyata T, Numa S. Primary structure of *Electrophorus electricus* sodium channel deduced from cDNA sequence. *Nature* 1984; 312:121-7.
4. Stuhmer W, Conti F, Suzuki H, Wang X, Noda M, Yahagi N, Kubo H, Numa S. Structural parts involved in activation and inactivation of the sodium channel. *Nature* 1989; 339:597-604.
5. Yang N, Horn R. Evidence for voltage-dependent movement in sodium channels. *Neuron* 1995; 15:213-6.
6. Yang N, George AL Jr, Horn R. Molecular basis of charge movement in sodium channels. *Neuron* 1996; 16:213-8.

7. Kontis KJ, Rounaghi A, Goldin AL. Sodium channel activation gating is affected by substitutions of voltage sensor positive charges in all four domains. *J Gen Physiol* 1997; 110:391-401.
8. Horn R, Ding S, Gruber HJ. Immobilizing the moving parts of voltage-gated ion channels. *J Gen Physiol* 2000; 116:69-89.
9. Cestele S, Yarov-Yarovoy V, Qu Y, Sampieri F, Scheuer T, Catterall WA. Structure and function of the voltage sensor of sodium channels probed by a β -scorpion toxin. *J Biol Chem* 2006; 281:21332-44.
10. Vassilev PM, Scheuer T, Catterall WA. Identification of an intracellular peptide segment involved in sodium channel inactivation. *Science* 1989; 241:1658-61.
11. West JW, Patton DE, Scheuer T, Wang Y, Goldin AL, Catterall WA. A cluster of hydrophobic amino acid residues required for fast Na⁺-channel inactivation. *Proc Natl Acad Sci USA* 1992; 89:10910-4.
12. Rohl CA, Boeckman FA, Baker C, Scheuer T, Catterall WA, Klevit RE. Solution structure of the sodium channel inactivation gate. *Biochem* 1999; 38:854-61.
13. Chahine M, George AL Jr, Zhou M, Ji S, Sun W, Barchi RL, Horn R. Sodium channel mutations in paramyotonia congenita uncouple activation from inactivation. *Neuron* 1994; 12:281-94.
14. Chen LQ, Santarelli V, Horn R, Kallen RG. A unique role for the S4 segment of domain 4 in the inactivation of sodium channels. *J Gen Physiol* 1996; 108:549-56.
15. Ji S, George AL Jr, Horn R, Barchi RL. Paramyotonia congenita mutations reveal different roles for segments S3 and S4 of domain D4 in hSkM1 sodium channel gating. *J Gen Physiol* 1996; 107:183-94.
16. Smith MR, Goldin AL. Interaction between the sodium channel inactivation linker and domain III S4-S5. *Biophys J* 1997; 73:1885-95.
17. Tang L, Kallen RG, Horn R. Role of an S4-S5 linker in sodium channel inactivation probed by mutagenesis and a peptide blocker. *J Gen Physiol* 1996; 108:89-104.
18. Lerche H, Peter W, Fleischhauer R, Pika-Hartlaub U, Malina T, Mitrovic N, Lehmann-Horn F. Role in fast inactivation of the IV/S4-S5 loop of the human muscle Na⁺ channel probed by cysteine mutagenesis. *J Physiol* 1997; 505:345-52.
19. McPhee JC, Ragsdale DS, Scheuer T, Catterall WA. A critical role for the S4-S5 intracellular loop in domain IV of the sodium channel α -subunit in fast inactivation. *J Biol Chem* 1998; 273:1121-9.
20. Mitrovic N, Lerche H, Heine R, Fleischhauer R, Pika-Hartlaub U, Hartlaub U, George AL Jr, Lehmann Horn F. Role in fast inactivation of conserved amino acids in the IV/S4-S5 loop of the human muscle Na⁺ channel. *Neurosci Lett* 1996; 214:9-12.
21. McPhee JC, Ragsdale DS, Scheuer T, Catterall WA. A critical role for transmembrane segment IVS6 of the sodium channel α subunit in fast inactivation. *J Biol Chem* 1995; 270:12025-34.

22. Green DS, George AL Jr, Cannon SC. Human sodium channel gating defects caused by missense mutations in S6 segments associated with myotonia. *J Physiol* 1998; 510:685-94.
23. Vedantham V, Cannon SC. Rapid and slow voltage-dependent conformational changes in segment IVS6 of voltage-gated Na⁺ channels. *Biophys J* 2000; 78:2943-58.
24. Mantegazza M, Yu FH, Catterall WA, Scheurer T. Role of the C-terminal domain in inactivation of brain and cardiac sodium channels. *Proc Natl Acad Sci USA* 2001; 98:15348-53.
25. Herzog RI, Liu C, Waxman SG, Cummins TR. Calmodulin binds to the C terminus of sodium channels Na_v1.4 and Na_v1.6 and differentially modulates their functional properties. *J Neurosci* 2003; 23:8261-70.
26. Motoike HK, Liu H, Glaaser IW, Yang A-S, Tateyama M, Kass RS. The Na⁺ channel inactivation gate is a molecular complex: a novel role of the COOH domain. *J Gen Physiol* 2004; 123:155-65.
27. Armstrong CM, Bezanilla F. Inactivation of the sodium channel II. Gating current experiments. *J Gen Physiol* 1977; 70:567-90.
28. Aldrich RW, Corey DP, Stevens CF. A reinterpretation of mammalian sodium channel gating based on single channel recording. *Nature* 1983; 7:436-41.
29. Bean BP. Sodium channel inactivation in the crayfish giant axon. *Biophys J* 1980; 35:595-614.
30. Armstrong CM. Na channel inactivation from open and closed states. *Proc Natl Acad Sci USA* 2006; 103:17991-6.
31. Lehmann Horn F, Engel AG, Ricker K, Rudel R. The periodic paralyses and paramyotonia congenita. In: *Myology*. Engel AG, Armstrong F, eds. New York: McGraw-Hill, 1994; 1303-4.
32. Cannon SC. Spectrum of sodium channel disturbances in the nondystrophic myotonias and periodic paralyses. *Kid Internatl* 2000; 57:772-9.
33. George AL Jr. Inherited disorders of voltage-gated sodium channels. *J Clin Invest* 2005; 115:1990-9.
34. Jurkat-Rott K, Lehmann-Horn F. Muscle channelopathies and critical points in functional and genetic studies. *J Clin Invest* 2005; 115:2000-9.
35. Yang N, Ji S, Zhou M, Ptacek LJ, Barchi RL, Horn R, George AL Jr. Sodium channel mutations in paramyotonia congenita exhibit similar biophysical phenotypes in vitro. *Proc Natl Acad Sci USA* 1994; 91:12785-9.
36. Ptacek LJ, George AL Jr, Barchi RL, Griggs RC, Riggs JE, Robertson M, Leppert MF. Mutations in an S4 segment of the adult skeletal muscle sodium channel cause paramyotonia congenita. *Neuron* 1992; 8:891-7.
37. Sasaki R, Takano H, Kamakura K, Kaida K, Hirata A, Saito M, Tanaka H, Kuzuhara S, Tsuji S. A novel mutation in the gene for the adult skeletal muscle sodium channel α -subunit (*SCN4A*) that causes paramyotonia congenita of von Eulenburg. *Arch Neurol* 1999; 56:692-6.
38. Richmond JE, Featherstone DE, Ruben PC. Human Na⁺ channel fast and slow inactivation in paramyotonia congenita mutants expressed in *Xenopus laevis* oocytes. *J Physiol* 1997; 499:589-600.
39. Bouhours M, Sternberg D, Davoine CS, Ferrer X, Willer JC, Fontaine N, Tabti N. Functional characterization and cold sensitivity of T1313A, a new mutation of the skeletal muscle sodium channel causing paramyotonia congenita in humans. *J Physiol* 2004; 554:635-47.
40. Bouhours M, Luce S, Sternberg D, Claude-Wilker J, Fontaine B, Tabti N. A1152D mutation of the Na⁺ channel causes paramyotonia congenita and emphasizes the role of DIII/S4-S5 linker in fast inactivation. *J Physiol* 2005; 565:415-27.
41. Fleischhauer R, Mitrovic N, Deymeer F, Lehmann-Horn F, Lerche H. Effects of temperature and mexiletine on the F1473S Na⁺ channel mutation causing paramyotonia congenita. *Pflugers Arch Eur J Physiol* 1998; 436:757-65.
42. Wu FF, Gordon E, Hoffman EP, Cannon SC. A C-terminal skeletal muscle sodium channel mutation associated with myotonia disrupts fast inactivation. *J Physiol* 2005; 565:371-80.
43. Featherstone DE, Fujimoto E, Ruben PC. A defect in skeletal muscle sodium channel deactivation exacerbates hyperexcitability in human paramyotonia congenita. *J Physiol* 1998; 506:627-38.
44. Groome JR, Fujimoto E, Ruben PC. The delay in recovery from fast inactivation in skeletal muscle sodium channels is deactivation. *Cell Mol Neurobiol* 2000; 20:521-7.
45. Dice MS, Abbruzzese JL, Wheeler JT, Groome JR, Fujimoto E, Ruben PC. Temperature-sensitive defects in paramyotonia congenita mutants R1448C and T1313M. *Muscle Nerve* 2004; 30:277-88.
46. Kuo CC, Bean BP. Na⁺ channels must deactivate to recover from inactivation. *Neuron* 1994; 12:819-29.
47. Cha A, Ruben PC, George AL Jr, Fujimoto E, Bezanilla F. Voltage sensors in domains III and IV, but not in I and II, are immobilized by Na⁺ channel fast inactivation. *Neuron* 1999; 22:73-87.
48. Groome JR, Larsen M, Coonts A. Deactivation defects in Na_v paramyotonia congenita mutations F1473S and F1705I. *Biophys Soc Abstr* 2007:467-Pos.
49. Groome JR, Dice MC, Fujimoto E, Ruben PC. Charge immobilization of skeletal muscle Na⁺ channels: role of residues in the III-IV inactivation linker. *Biophys J* 2007; 93:1519-33.
50. Kuhn FJP, Greef NG. Movement of voltage sensor S4 in domain 4 is tightly coupled to sodium channel fast inactivation and gating charge immobilization. *J Gen Physiol* 1999; 114:167-83.
51. Rhodes TH, Lossin C, Vanoye CG, Wang DW, Carniciu S, Devinsky O, George AL Jr. Non-inactivating voltage-gated sodium channels in severe myoclonic epilepsy of infancy. *Proc Natl Acad Sci USA* 2004; 101:11147-52.
52. Filatov GN, Nguyen TP, Kraner SD, Barchi RL. Inactivation and secondary structure in the D4/S4-5 region of the SkM1 sodium channel. *J Gen Physiol* 1998; 111:703-15.
53. Popa MO, Alekov AK, Bail S, Lehmann-Horn F, Lerche H. Cooperative effect of S4-S5 loops in domains D3 and D4 on fast inactivation of the Na⁺ channel. *J Physiol* 2004; 561:39-51.
54. Chanda B, Bezanilla F. Tracking voltage-dependent conformational changes in skeletal muscle sodium channel during activation. *J Gen Physiol* 2002; 120:629-45.
55. Sheets MF, Kyle JW, Kallen RG, Hanck DA. The Na channel voltage sensor associated with inactivation in localized to the external charged residues of domain IV, S4. *Biophys J* 1999; 77:747-57.
56. Tang L, Chehab N, Wieland SJ, Kallen RG. Glutamine substitution at alanine¹⁶⁴⁹ in the S4-S5 cytoplasmic loop of domain 4 removes the voltage sensitivity of fast inactivation in the human heart sodium channel. *J Gen Physiol* 1998; 111:639-52.
57. Spanpanato J, Kearney JA, de Haan G, McEwen DP, Escayg A, Aradi L, MacDonald BT, Levin SI, Soltesz I, Benna P, Montalenti E, Isom LL, Goldin AL, Meisler MH. A novel epilepsy mutation in the sodium channel *SCN1A* identifies a cytoplasmic domain for β subunit interaction. *J Neurosci* 2004; 24:10022-34.
58. Dougherty K, De Santiago-Castillo JA, Covarrubias M. Gating charge immobilization in K_v4.2 channels: the basis of closed-state inactivation. *J Gen Physiol* 2008; 131:257-73.

